



Article

Treatment of Bio-Treated Coking Wastewater by Catalytic Ozonation with Semi-Batch and Continuous Flow Reactors

Can He ^{1,2}, Jianbing Wang ^{1,2,*}, Heng Xu ^{1,2}, Xiangyu Ji ¹, Weiyi Wang ¹ and Xieyang Xu ¹

¹ School of Chemical and Environmental Engineering, China University of Mining and Technology (Beijing), D11 Xueyuan Road, Haidian District, Beijing 100083, China; hecan086@163.com (C.H.); xuheng@cumtb.edu.cn (H.X.); jxy781935408@163.com (X.J.); 18811020418@163.com (W.W.); xuxy_env@163.com (X.X.)

² State Key Laboratory of Coal Resource and Safe Mining, China University of Mining and Technology (Beijing), Beijing 100083, China

* Correspondence: wangjb@cumtb.edu.cn; Tel.: +86-136-9331-4626

Received: 12 August 2020; Accepted: 7 September 2020; Published: 10 September 2020



Abstract: In this work, the treatment of bio-treated coking wastewater (BCW) by catalytic ozonation was conducted in semi-batch and continuous flow reactors. The kinetics of chemical oxygen demand (COD) removal were analyzed using BCWs from five coking plants. An integral reactor with catalytic ozonation stacked by ozone absorption (IR) was developed, and its efficiency was studied. The catalyst of $Mn_xCe_{1-x}O_2/\gamma-Al_2O_3$ was efficient in the catalytic ozonation process for the treatment of various BCWs. The chemical oxygen demand (COD) removal efficiencies after 120 min reaction were 64–74%. The overall apparent reaction rate constants were 0.0101–0.0117 min^{-1} , which has no obvious relationship with the initial COD of BCW and pre-treatment biological process. The IR demonstrated the highest efficiency due to the enhancement of mass transfer and the utilization efficiency of ozone. Bypass internal circulation can further improve the reactor efficiency. The optimal results were obtained with the ozone absorption section accounting for 19% of the valid water depth in the reactor and 250% of circulation flow ratio. The long-term and full-scale application of the novel reactor in a continuous mode indicated stable removal of COD and polycyclic aromatic hydrocarbons (PAHs). The results showed that the system of IR is a promising reactor type for tertiary treatment of coking wastewater by catalytic ozonation.

Keywords: catalytic ozonation; coking wastewater; rate constant; reactor; polynuclear aromatic hydrocarbons

1. Introduction

Coking wastewater is a type of typical complex industrial wastewater, in which significant amounts of toxic compounds such as polynuclear aromatic hydrocarbons (PAHs), cyanides, and high concentrations of ammonium salts and chlorides are present [1,2]. Generally, coking wastewater has been effectively treated by the conventional biological treatment process. However, the chemical oxygen demand (COD) values of the conventional biological treated coking wastewater are generally above $150 \text{ mg}\cdot\text{L}^{-1}$, and most organic compounds in the effluent are refractory, toxic, mutative, and carcinogenic [3]. The discharge of the bio-treated coking wastewater (BCW) without effective further treatment could result in serious environmental problems. Thus, efforts on advanced treatment processes for coking wastewater to remove the organic matters present in the BCW, especially refractory and toxic compounds, are necessary to guarantee the safety of the water environment [3,4].

Various methods such as coagulation, flocculation, adsorption, and advanced oxidation have been studied to remove the organic matters present in the BCW [5,6]. Among them, ozonation as a follow-up process of a biological process is widely used in the treatment of BCW. However, more toxic compounds may be produced during the ozonation [7]. Ozonation is also not efficient for the degradation of some recalcitrant compounds. To overcome the limitation of ozonation, catalytic ozonation was developed for the removal of refractory or toxic organic pollutants in water, which can be conducted under ambient conditions and may be easily applied without any auxiliary thermal, light, or high-pressure systems [8–10]. Recently, catalytic ozonation has shown high efficiency in the removal of recalcitrant and toxic organic pollutants [11–14] and the tertiary treatment of some industrial wastewater [15,16].

During catalytic ozonation, catalysts play an important role in the production of hydroxyl radicals and the degradation of pollutants [17]. Over the past two decades, a lot of efficient catalysts have been developed [5,18,19]. Among them, the Mn–Ce–O catalyst showed high total organic carbon degradation for phenolic wastewater [20] and high mineralization degrees for carboxylic acids [21], sulfanilic acid, and aniline [22] in catalytic ozonation. Additionally, Ceria (CeO_2) can reduce bromate formation during ozonation [23,24]. However, most of these catalysts are powdery nanosized particles, which are difficult to recycle after being used, thereby remarkably limiting their practical application [25]. Due to the lack of suitable pellet catalysts, few studies reported about the practical application of catalytic ozonation for the treatment of actual wastewater in a continuous reactor. Recently, there have been some reports on the long-term application of millimetric spherical catalysts in catalytic ozonation for the advanced treatment of actual wastewater. Wei et al. [26] investigated the long-term catalytic ozonation with the CuCo/NiCAF catalyst for the treatment of coal-gasification wastewater. The results demonstrated that the catalyst showed excellent catalytic activity and structural stability for practical application. In our previous study [27], a long-term pilot-scale and full-scale study on the advanced treatment of coking wastewater by catalytic ozonation with an $\text{Mn}_x\text{Ce}_{1-x}\text{O}_2/\gamma\text{-Al}_2\text{O}_3$ catalyst were carried out. It was found that backflushing significantly improved COD removal stability in the catalytic ozonation process. All these studies make it possible to popularize the catalytic ozonation process on a large scale. However, most of the current research is still focused on the development of novel high-efficient catalysts, and there are few reports on the reactor and the kinetics for actual wastewater. It is well known that catalytic ozonation is a three-phase reaction, in which the mass transfer of ozone plays an important role. Optimizing the reactor structure is a possible alternative for the improvement of the ozone mass transfer efficiency. Additionally, the kinetic rate parameters of actual wastewater can be used to provide reference and guidance for the design and operation of the catalytic ozonation process.

In this study, the treatments of bio-treated coking wastewater with different reactors were conducted to investigate their characteristics of ozone mass transfer. A novel integral reactor with catalytic ozonation stacked by ozone absorption (IR) was developed based on the experiments, and the parameters of the reactor structure were optimized. The 487 days of engineering application with the novel reactor were performed, and the removals of typical pollutants, i.e., polycyclic aromatic hydrocarbons (PAHs), which are strictly regulated by the discharge standard in China, were examined in the long-term operation. Additionally, the kinetics of COD degradation in different coking wastewater were explored with the novel reactor.

2. Experimental

2.1. Catalyst Synthesis and Characterization

The raw materials for catalyst synthesis, including Cerium nitrate hexahydrate and Manganese nitrate (50% solution) with analytic grade, were obtained from Macklin Biochemical Co., Ltd. (Shanghai, China). The commercial millimetric spherical $\gamma\text{-Al}_2\text{O}_3$ (Shandong, China) was washed with water and subsequently dried at 378 K for 4 h before use.

The $Mn_xCe_{1-x}O_2/\gamma-Al_2O_3$ catalyst was prepared by impregnation-calcination as described by He et al. [27]. Upon impregnation and calcination, the $\gamma-Al_2O_3$ spheres were converted into a $Mn_xCe_{1-x}O_2/\gamma-Al_2O_3$ shell/core structure.

The N_2 adsorption-desorption isotherms were carried out on a Micromeritics ASAP2460 apparatus to measure the surface area, pore volume, and pore size of the support and the catalyst. The SEM images and EDS mapping profiles were collected on a cold field emission SEM SU8020 (Hitachi, Japan) equipped with EDS EX250 (Horiba, Japan). X-ray diffraction (XRD) analyses were made on a D8 Advance instrument (Bruker, German) in the 2θ range from 5° to 90° (scan rate $4^\circ/\text{min}$) with a $Cu K\alpha$ radiation source ($\lambda = 1.5406 \text{ \AA}$). The loading amounts of the Mn and Ce were quantified by ICP-OES (ICP-OES730, Agilent, CA, USA), in which the catalyst was digested with aqua regia at a maximum temperature of 200°C prior to analysis.

2.2. Wastewater Characteristics

The BCW were collected from five coking plants. The characteristics of those BCW and bio-treatment processes in different coking plants are depicted in Table 1.

Table 1. Characteristics of bio-treated coking wastewater (BCW) and bio-treatment processes in different coking plants.

Plant ‡	Biological Pre-Treatment		Characteristics of BCW		
	Process	Scale ($\text{m}^3 \cdot \text{h}^{-1}$)	COD ($\text{mg} \cdot \text{L}^{-1}$)	PH	ORP [§] (mV)
B-A	A/O	200	172–188	7.87–8.11	153–229
B-M	A/O/MBR pilot	10	196–258	7.87–8.11	211–229
F	A/A/O	380	140–195	7.15–8.35	71.6–194.3
A	A/A/O	50	104–137	7.0–9.0	160–210
J	A/A/O/MBBR	80	114–160	8.47–9.47	155–273
X	A/A/O	100	260–319	7.0–8.0	220–250

‡ Plant B is in east China (Both B-A and B-M belong to plant B, the raw coking wastewater was the same but the biological pre-treatment process was different), plant F is in the northwest China, plant A is in the northeast China, plant J and plant X are in the north China. § ORP, oxidation-reduction potential.

2.3. Experimental Procedure

The treatments of BCW from the five coking plants were investigated in semi-batch test mode using an integral reactor with catalytic ozonation stacked by ozone absorption (IR) setup. A schematic diagram for the catalytic ozonation process using IR setup is shown in Figure 1. The $Mn_xCe_{1-x}O_2/\gamma-Al_2O_3$ of 72 kg catalyst was loaded into a $\phi 650 \text{ mm} \times 2200 \text{ mm}$ reactor made of SUS316L stainless steel before the experiment and the height of catalyst bed was 0.31 m. In the semi-batch test, 600 L of BCW was loaded with a diaphragm pump into the reactor at the beginning of the experiment. During the experiment, the circulating pump worked continuously to circulate wastewater from the top to the bottom of the reactor. Ozone gas generated by a CF-G-2-100g ozone generator (Guolin Technology, Qingdao, China) with dry pure oxygen was continuously fed into the reactor through a $40 \mu\text{m}$ cylindrical microporous titanium plate at the bottom of the reactor. Residual ozone gas from the reactor was destroyed in vent ozone destructor. Samples were collected at predetermined intervals. The parallel experiments of adsorption on the catalysts (without ozone) and single ozonation (without catalysts) were conducted under identical conditions.

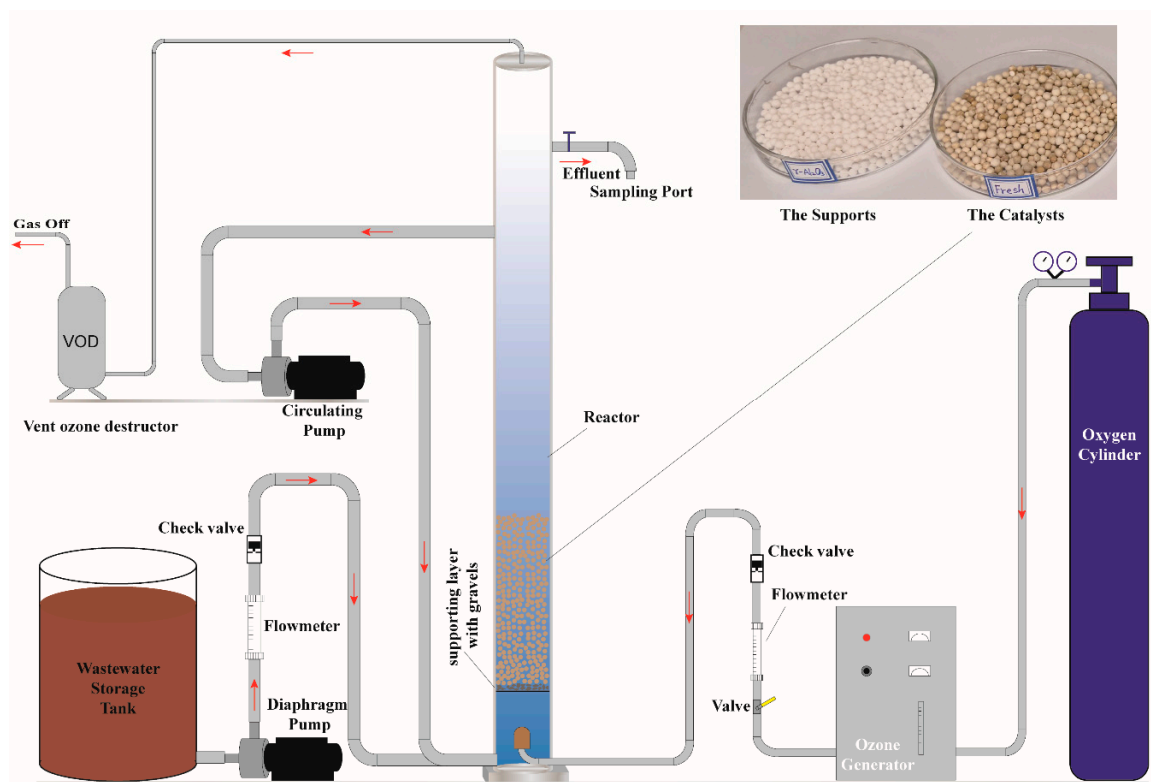


Figure 1. Schematic diagram of catalytic ozonation process for the pilot experiments.

The continuous flow experiments of catalytic ozonation were carried out in four types of reactors. They are the three-phase bypass internal circulation reactor (TR), sequential flow series reactor (SR), the gas-liquid countercurrent reactor (CR), and an integral reactor with catalytic ozonation stacked by ozone absorption (IR), respectively. The structure of each reactor is shown in Figure 2. In each reactor, the $Mn_xCe_{1-x}O_2/\gamma-Al_2O_3$ catalyst was added for $180\text{ g}\cdot\text{L}^{-1}$ of catalyst dosage. The total effective volumes of the reactors are 600 L, and BCW was continuously pumped into each reactor at a wastewater flux of $400\text{ L}\cdot\text{h}^{-1}$. The generation and supply mode of ozone gas was the same as that of the semi-batch experiment. Ozone dosage was the same for each reactor and it was controlled at the desired amount by adjusting gas flux and ozone generator power.

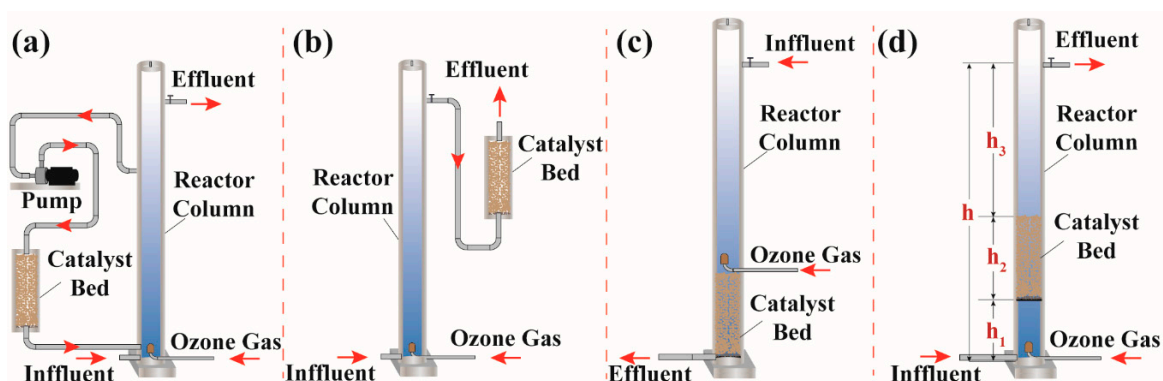


Figure 2. Catalytic ozonation reactors, (a) the three-phase bypass internal circulation reactor (TR), (b) the sequential flow series reactor (SR), (c) the gas-liquid countercurrent reactor (CR), and (d) the integral reactor with catalytic ozonation stacked by ozone absorption (IR).

As depicted in Figure 2d, the IR has two sections, i.e., ozone absorption section and catalytic ozonation section consisted of catalyst bed and catalytic reaction section. The height of the ozone

absorption section, catalyst bed, catalytic reaction section, and the valid water depth in the reactor was defined as h_1 , h_2 , h_3 , and h , respectively. In this work, the h_2 was 0.31 m. To further optimize the structure parameters, different heights of the ozone absorption section (h_1) were set to conduct continuous catalytic ozonation for the treatment of BCW, and the COD removal efficiencies were investigated. For the inhibition of channeling and the further enhancement of mass transfer, a circulating pump was used in the reactor for the bypass internal circulating of BCW, and the effect of the circulation flow ratios (R) on process efficiency was studied. The R value was calculated as follows (Equation (1)),

$$R = \frac{\int Q_c \times dt}{\int Q_1 \times dt} \quad (1)$$

where Q_1 and Q_c are the influent water flux ($L \cdot h^{-1}$) and the circulation flux ($L \cdot h^{-1}$) in the system, respectively, t is time (min).

The long-term continuous catalytic ozonation for the treatment of BCW was conducted with the full-scale IR system. The COD removal during the long-term operation was investigated in our previous study [27], but the removal of organic compounds in different running times was not studied. Thus, the 16 PAHs present in the influent and the effluent of IR system were analyzed on day 15 and 487 of operation, respectively. Additionally, the three-dimensional excitation-emission matrix fluorescence (3DEEM) and the ultraviolet absorbance at 254 nm (UV254) were monitored. The parameters of the full-scale application system are the same as those of the previous study [27].

All the experiments were repeated at least three times, and all the data are the average of these determinations.

The ozone utilization efficiency ($\Delta O_3/\Delta COD$) was calculated as follows (Equation (2)),

$$\Delta O_3/\Delta COD = \frac{\int Q_g \times ([O_3]_{in} - [O_3]_{out})dt - \int Q_1 \times [O_3]_{aqs}dt}{\int Q_1 \times (COD_0 - COD_t)dt} \quad (2)$$

where $[O_3]_{in}$, $[O_3]_{out}$, and $[O_3]_{aqs}$ are the ozone content ($mg \cdot L^{-1}$) in the inlet gas, the outlet gas, and the effluent water, respectively, and Q_g is the inlet gas flux ($L \cdot h^{-1}$) of the reactor, and COD_0 and COD_t represent the COD content ($mg \cdot L^{-1}$) in the influent water and the effluent water, respectively. The $[O_3]_{out}$ was assumed to be ~ 0 as its value was generally very small in the IR system and it was difficult to be detected continuously and effectively. The $[O_3]_{aqs}$ was approximate ~ 0 under the optimized ozone dosage. Thus, the ozone-utilization efficiency could be defined as the ozone consumption ($mg \cdot L^{-1}$) per unit of removed COD ($mg \cdot L^{-1}$) [27].

2.4. Analytic Methods

The concentration of COD was measured using the dichromate method (HJ 828-2017 China). The UV254 was monitored with a 752 UV/Vis spectrophotometer (Shanghai, China). The pH and ORP were analyzed using a multiparameter meter (HACH sensION+ MM374, Loveland, CO, USA). The 3DEEM was obtained with a fluorometer (Hitachi F-7000 FL, Hitachi, Tokyo, Japan). The PAHs were assayed using GC-MS (Shimadzu QP2010-Ultra) by capillary column DB-5MS ($30 \text{ m} \times 0.25 \text{ mm} \times 0.25 \text{ } \mu\text{m}$, Agilent, J&W Scientific); GC oven was kept at $70 \text{ }^\circ\text{C}$ for 2 min, then increased to $320 \text{ }^\circ\text{C}$ at $10 \text{ }^\circ\text{C} \cdot \text{min}^{-1}$, and finally held at $320 \text{ }^\circ\text{C}$ for 6 min. The ozone concentration in the gas phase was measured by iodometric method [28], and the dissolved ozone in liquid phase was determined with the indigo method [29].

3. Results and Discussions

3.1. Catalyst Characterization

Table 2 shows the physico-chemical properties of the γ -Al₂O₃ and Mn_xCe_{1-x}O₂/ γ -Al₂O₃ catalyst. A decrease in BET area and pore volume of the support was resulted from the deposition of MnO_x and CeO_x, indicating that the supported metal occupied the pores of the support [30]. However, the Mn_xCe_{1-x}O₂/ γ -Al₂O₃ catalyst kept the mesoporous structure of γ -Al₂O₃. The mesoporous structure of the millimetric sphere is desirable since it can balance large surface area with rapid intraparticle diffusion [31,32].

Table 2. Physico-chemical properties of the support and catalyst.

Sample	BET Area (S _{BET} /m ² ·g ⁻¹)	Mesopore Volume (V _{mes} /cm ³ ·g ⁻¹)	Total Pore Volume (V _{0.995} /cm ³ ·g ⁻¹)	Average Pore Diameter (nm)
γ -Al ₂ O ₃	214.2	0.373	0.385	7.2
Mn _x Ce _{1-x} O ₂ / γ -Al ₂ O ₃	195.0	0.363	0.364	7.5

Figure 3 presents the XRD results of the support and fresh catalyst. Four broad peaks in the XRD pattern of γ -Al₂O₃ are observed at ca. 19.5°, 37.4°, 45.9°, 66.9°, representing the crystalline phase of γ -Al₂O₃ (JCPDS 46-1131), which is similar to that obtained by Bing et al. [33]. The diffraction peaks near 16.5°, 37°, and 45° in the XRD pattern of the Mn_xCe_{1-x}O₂/ γ -Al₂O₃ catalyst are conformed to tetragonal MnO₂ (JCPDS 42-1169), and the peaks around 28.5° and 46° are attributed to CeO₂ (JCPDS 43-1002) [34]. The results showed that both Mn and Ce oxides existed in the catalyst.

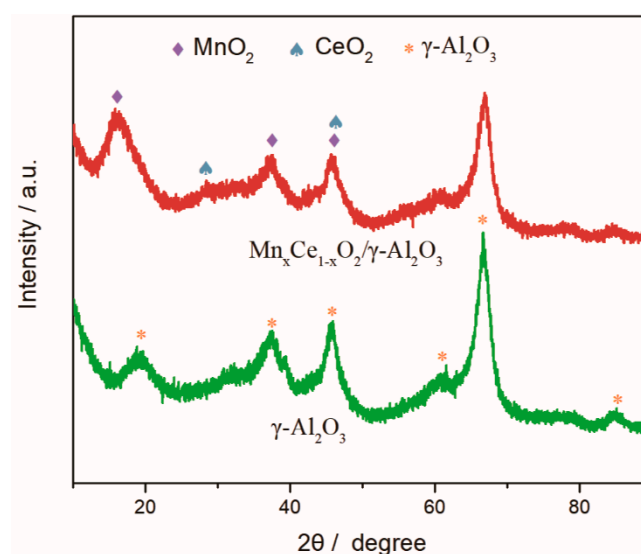


Figure 3. XRD patterns of γ -Al₂O₃ and Mn_xCe_{1-x}O₂/ γ -Al₂O₃.

The Mn_xCe_{1-x}O₂/ γ -Al₂O₃ catalyst is a porous beige pellet (Figure 1) and covered by closely packed globular particles (Figure 4c,f), while the γ -Al₂O₃ support is a porous white pellet (Figure 1, Figure 4a). The core/shell structure of γ -Al₂O₃@Mn_xCe_{1-x}O₂ pellet (3.0–5.0 mm in diameter) with an out-layer thickness of ~622 μ m could easily be confirmed (Figure 4e). Previous studies have shown that core-shell structures can enhance metal-support interactions between the core and shell components by maximizing this interface, thereby providing advanced materials for catalytic applications [35]. The diameter of the pore is about 1–3 μ m, and the diameter of the particles is less than ~25 nm.

EDS analysis (Figure 4b,d) demonstrates that the elemental composition of materials on the γ -Al₂O₃ support was mainly Al and O, while the Mn_xCe_{1-x}O₂/ γ -Al₂O₃ catalyst was composed

of Al, Mn, Ce, and O. According to the analysis of ICP-OES, the loadings of Mn and Ce in the $Mn_xCe_{1-x}O_2/\gamma-Al_2O_3$ catalyst were 1.42 wt.% and 1.22 wt.%, respectively.

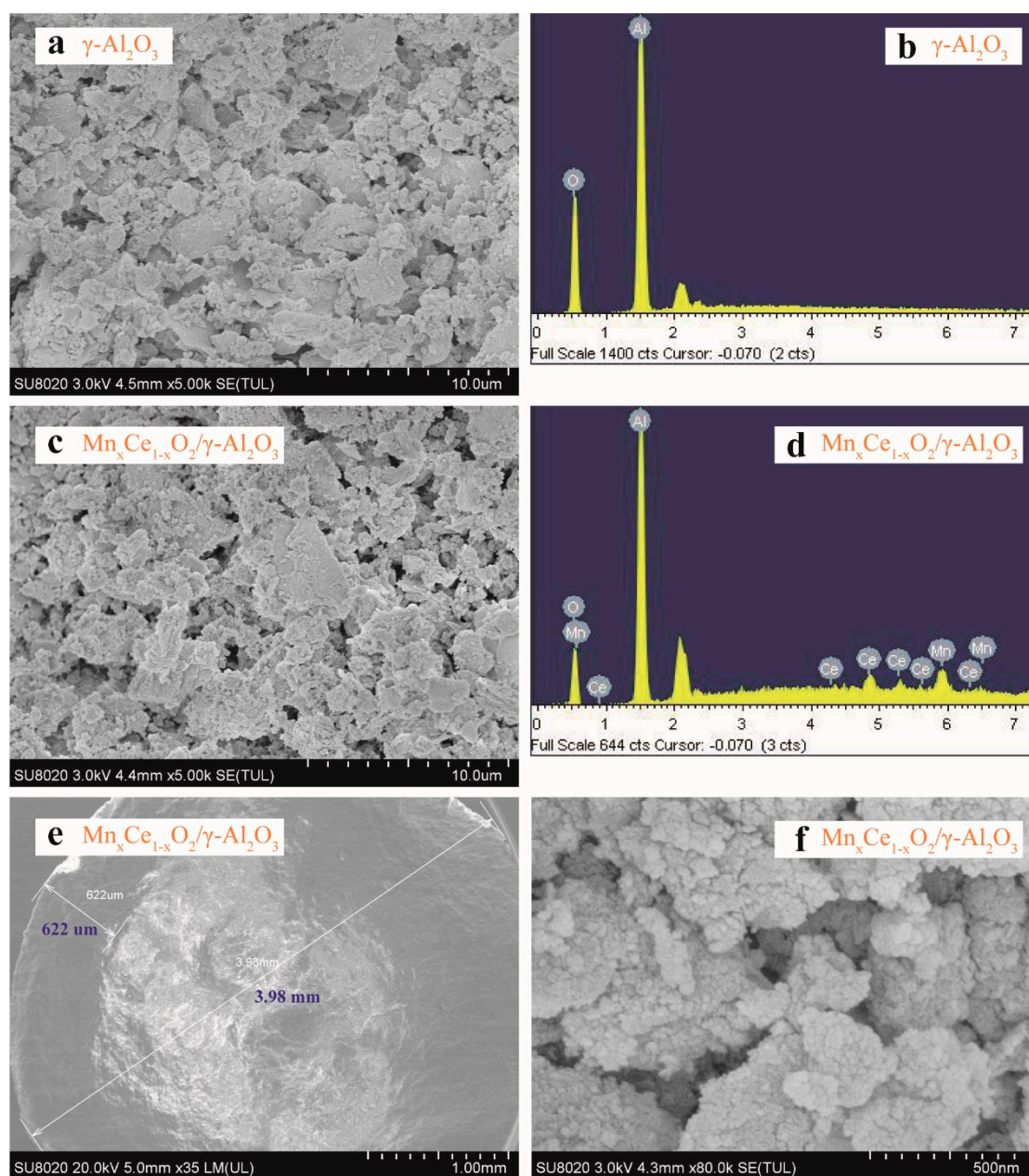


Figure 4. SEM and EDS analysis results: (a) SEM of $\gamma-Al_2O_3$ support, (c,e,f) SEM of $Mn_xCe_{1-x}O_2/\gamma-Al_2O_3$ catalyst, (b) EDS of $\gamma-Al_2O_3$ support, (d) EDS of $Mn_xCe_{1-x}O_2/\gamma-Al_2O_3$ catalyst.

3.2. Treatment of BCW with Semi-Batch Reactor

Figure 5 shows the results for the treatment of BCW from the five coking plants by various processes. The COD removal by adsorption was very low for all the BCWs. Only 14.5%–20% of COD was eliminated by single ozonation after 120 min. However, 64%–74% of COD was removed by the catalytic ozonation for 120 min. Thus, the COD removal was mainly owing to catalytic ozonation rather than adsorption of the catalyst. In our previous study [27], the data of 12-month operation showed that the average concentrations of Mn and Ce leached from the catalyst were 8.35 and 0.42 $\mu g \cdot L^{-1}$, respectively, implying that the homogeneous catalytic oxidation of the leaching active components could be ignored.

$\Delta O_3/\Delta COD$ for the treatments of various BCW by catalytic ozonation are also presented in Figure 5. The ratios ranged from 0.9 to 5.13. When the COD content of BCW was 150–220 $\text{mg}\cdot\text{L}^{-1}$ with 64–75% of the COD removal efficiency, the $\Delta O_3/\Delta COD$ ratio was generally in the range of 2.1–2.6 for 120 min of catalytic ozonation. For plant F, although the COD content of BCW was about 188 $\text{mg}\cdot\text{L}^{-1}$, the ratio was 1.2, which might be related to the low ORP of the BCW since wastewater with low ORP was more easily oxidized. However, when the COD removal efficiency was 68–70%, the ozone consumption was lower for the BCW with more than 300 $\text{mg}\cdot\text{L}^{-1}$ initial COD; the ozone consumption was higher for the BCW with less than 120 $\text{mg}\cdot\text{L}^{-1}$ initial COD. Thus, the ratio for plant A was the maximum, while the value for plant X was the minimum. These also indicated that more ozone was consumed for the removal of per unit COD with less than 120 $\text{mg}\cdot\text{L}^{-1}$ of initial COD concentration and more than 65% of removal efficiency.

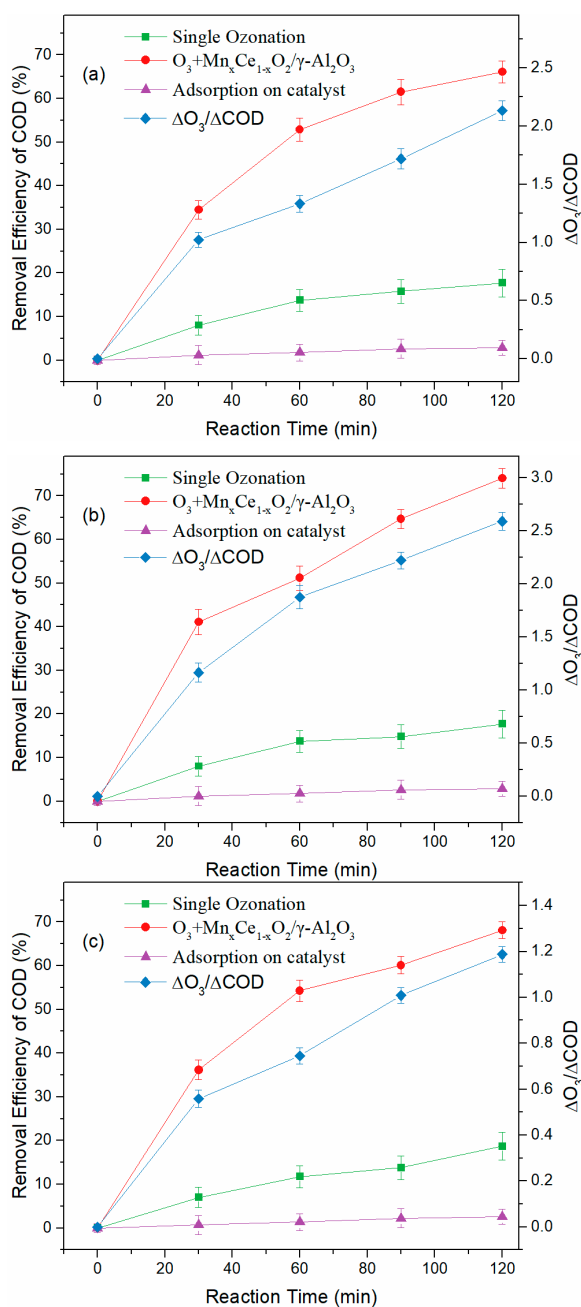


Figure 5. Cont.

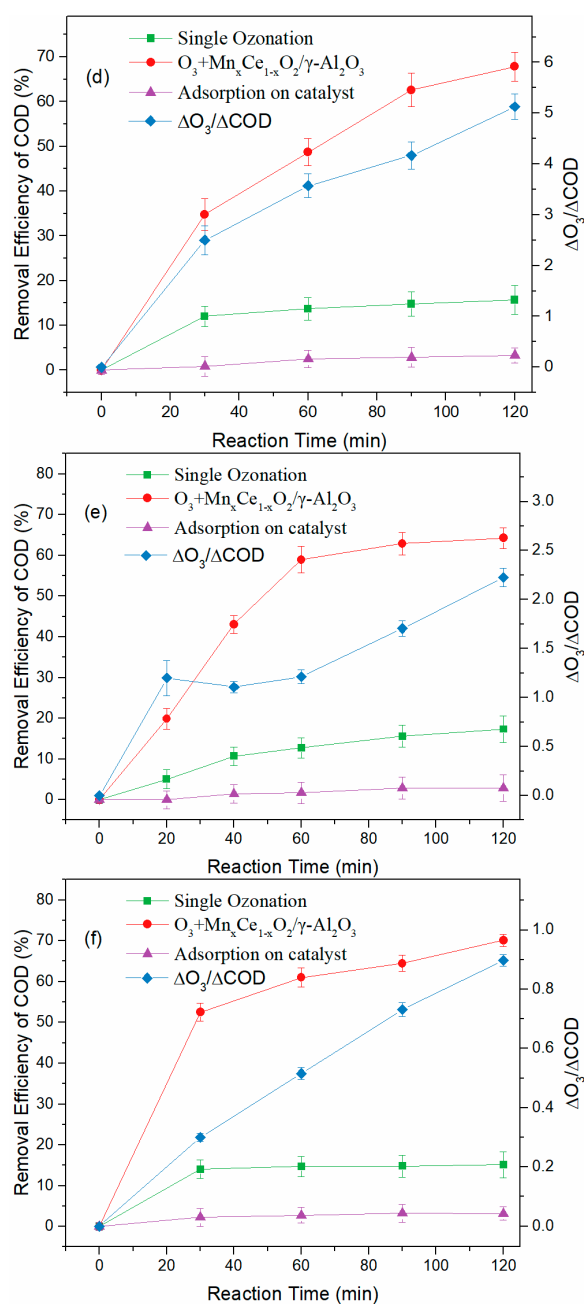


Figure 5. $\Delta O_3/\Delta$ chemical oxygen demand (COD) values during catalytic ozonation of BCW and COD removal efficiency in different process for the treatment of BCW from (a) B-A, (b) B-M, (c) F, (d) A, (e) J, and (f) X plant. (Experimental conditions: catalyst dosage, $180 \text{ g}\cdot\text{L}^{-1}$; ozone dosage, (a) $120 \text{ mg}\cdot\text{L}^{-1}\cdot\text{h}^{-1}$, (b) $210 \text{ mg}\cdot\text{L}^{-1}\cdot\text{h}^{-1}$, (c) $76 \text{ mg}\cdot\text{L}^{-1}\cdot\text{h}^{-1}$, (d) $200 \text{ mg}\cdot\text{L}^{-1}\cdot\text{h}^{-1}$, (e) $108 \text{ mg}\cdot\text{L}^{-1}\cdot\text{h}^{-1}$, and (f) $100 \text{ mg}\cdot\text{L}^{-1}\cdot\text{h}^{-1}$; COD of influent, (a) $176.5 \pm 4.5 \text{ mg}\cdot\text{L}^{-1}$, (b) $218 \pm 20 \text{ mg}\cdot\text{L}^{-1}$, (c) $188 \pm 7.0 \text{ mg}\cdot\text{L}^{-1}$, (d) $115 \pm 11 \text{ mg}\cdot\text{L}^{-1}$, (e) $151 \pm 8.5 \text{ mg}\cdot\text{L}^{-1}$, and (f) $315 \pm 4.0 \text{ mg}\cdot\text{L}^{-1}$).

Due to the complex composition of actual coking wastewater, it was not appropriate to analyze the kinetics using a single representative pollutant. Therefore, the apparent kinetics of COD degradation were studied. The COD removal in catalytic ozonation process can be attributed to the direct reaction with molecular ozone, indirect reaction with generated OH, and adsorption of pollutants on the catalyst

surface. Combined with our previous research [36], the concentration profiles of COD can be simplified described with the Equation (3).

$$\frac{d[\text{COD}]}{dt} = -k_1 C_{\text{O}_3\text{L}}[\text{COD}] - k_2 C_{\text{OH}}[\text{COD}] - k_a m[\text{COD}] \quad (3)$$

Equation (3) was integrated to give:

$$\ln \frac{[\text{COD}]_t}{[\text{COD}]_0} = -(k_1 C_{\text{O}_3\text{L}} + k_2 C_{\text{OH}} + k_a m)t = -kt \quad (4)$$

where k_1 , k_2 , k_a , and k represent the rate constant of the reaction of ozone with COD ($\text{L}\cdot\text{mol}^{-1}\cdot\text{s}^{-1}$), the rate constant of the reaction between hydroxyl radical and COD ($\text{L}\cdot\text{mol}^{-1}\cdot\text{s}^{-1}$), the capacity mass transfer coefficient of the catalyst ($\text{s}^{-1}\cdot\text{g}^{-1}$), and the overall apparent reaction rate constant of COD removal (min^{-1}), respectively; $C_{\text{O}_3\text{L}}$ is the ozone content in the aqueous solution ($\text{mg}\cdot\text{L}^{-1}$); C_{OH} is the $\cdot\text{OH}$ content in the liquid phase ($\text{mg}\cdot\text{L}^{-1}$); m is the mass of the catalyst (g); $[\text{COD}]_0$ and $[\text{COD}]_t$ are the COD concentration at time zero and any time t (min), respectively.

Therefore, plotting $-\ln([\text{COD}]_t/[\text{COD}]_0)$ versus the reaction time, would yield overall apparent reaction rate constants for COD removal in the catalytic ozonation process. For comparison, the overall apparent reaction rate constants of COD removal in BCW by single ozonation were also calculated by the same method. The results are summarized in Table 3. The overall apparent reaction rate constants for COD removal were 0.0101–0.0117 min^{-1} for the five types of BCW, which were 2.9–3.5 times of a single ozonation system (0.0034 min^{-1}). They were lower than those achieved in the treatment of bio-treated tannery wastewater by catalytic ozonation (0.0328 min^{-1}) and single ozonation (0.0141 min^{-1}) [37], indicating that the BCW used in this study was more difficult to degrade than the bio-treated tannery wastewater used in the reference. These results also showed that overall apparent reaction rate constant k has nothing to do with the initial COD of BCW and pre-treatment biological process. Additionally, the reaction rate constant also has no relationship with the ozone dosage when ozone is sufficient. Taking BCW from B-M as an example (Figure 6), the reaction rate constant was relatively small when the ozone dosage was 90 $\text{mg}\cdot\text{L}^{-1}$ or 120 $\text{mg}\cdot\text{L}^{-1}$, while the reaction rate constant was about 0.011 when the ozone dosage was 195 $\text{mg}\cdot\text{L}^{-1}$, 210 $\text{mg}\cdot\text{L}^{-1}$, or 275 $\text{mg}\cdot\text{L}^{-1}$. Hence, when the ozone dosage is not enough, the dissolved ozone in aqueous liquid cannot be replenished in time, so the ozone dosage is a limiting factor for the catalytic ozonation reaction. When the ozone dose is sufficient, the mass transfer of ozone plays an important role. Based on the results of the semi-batch test, when the ozone dosages were 195, 210, and 275 $\text{mg}\cdot\text{L}^{-1}$, the operating costs were USD 3.99, USD 4.16, and USD 5.46 (kgCOD^{-1}), respectively. Thus, the optimal ozone dosage for plant B-M was 210 $\text{mg}\cdot\text{L}^{-1}$ after considering efficiency and cost-effectiveness. The ozone dosages for other coking plants in this study were the optimal ozone dosages based on this principle. The constant k given in this paper is valuable for the design and operation of the catalytic ozonation process.

Table 3. Kinetic constants of COD removal by the catalytic ozonation or single ozonation system.

	Catalytic Ozonation						Single Ozonation
	B-A	B-M	F	J	A	X	
$k (\times 10^{-3} \text{min}^{-1})$	10.13	11.65	10.30	10.40	10.20	11.65	3.4
Correlation coefficient (R^2)	0.9757	0.9881	0.9767	0.9460	0.9870	0.9210	0.9860

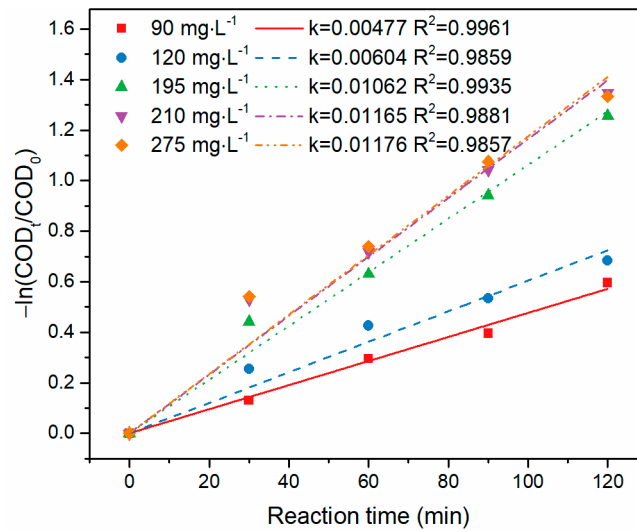


Figure 6. The effect of ozone dosage on the reaction rate constants.

3.3. Treatment of BCW in Various Continuous Flow Reactor

Figure 7a shows the COD removal efficiencies for the treatment of BCW using different reactors. The COD removal efficiencies in TR, SR, CR, and IR were 37.4%, 24.6%, 33.4%, and 48.1%, respectively. The $\Delta O_3/\Delta COD$ ratios corresponding to them were 2.14, 3.25, 2.40, and 1.67. Thus, the performance of the IR was significantly better than the other three reactors.

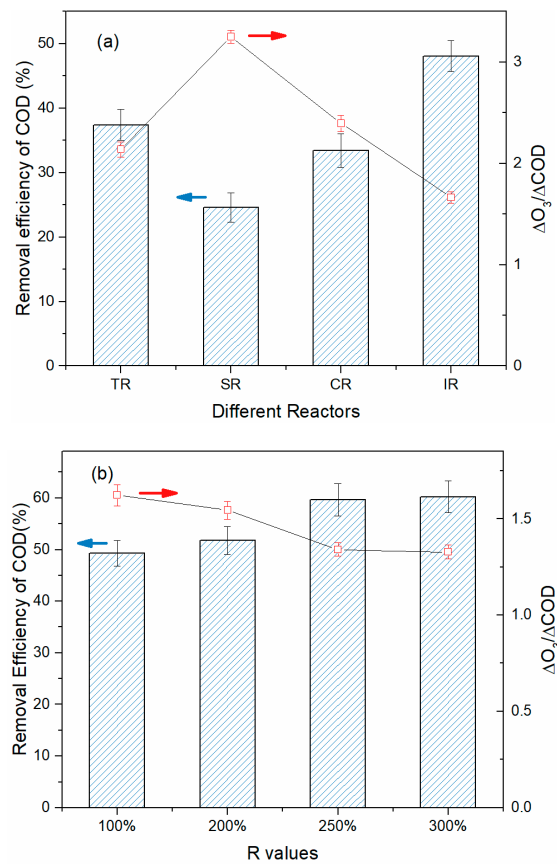


Figure 7. The effect of (a) different reactors and (b) circulation flow ratios (experimental conditions: pH, 8.5 ± 0.3 ; catalyst dosage, $180 \text{ g}\cdot\text{L}^{-1}$; ozone dosage, $80 \text{ mg}\cdot\text{L}^{-1}\cdot\text{h}^{-1}$; COD of influent, $\sim 150 \text{ mg}\cdot\text{L}^{-1}$, hydraulic retention time, 90 min).

In the system of IR, ozone firstly entered the ozone absorption section. It would react rapidly with some organic pollutants in the BCW, thereby the absorption of ozone could be enhanced in the reaction. In the ozone absorption section, the mass transfer of ozone would not be affected by the catalyst. Therefore, bubble coalescence was not significant. Small bubbles were favorable for ozone absorption. When the dissolved ozone entered into the catalyst bed, it was transformed into hydroxyl radicals and reactive oxygen species with the catalytic effect of $Mn_xCe_{1-x}O_2/\gamma-Al_2O_3$. The consumed ozone could be replenished by the dissolved ozone in the up-flow. The hydroxyl radicals or reactive oxygen species generated in the solution and the remained ozone continued to react with organic pollutants in the catalytic reaction section. Since ozone absorption could be enhanced by a chemical reaction in the absorption section and the ozone consumed in the catalytic ozonation section could be replenished in time, the system of IR could obtain high efficiency.

In the TR, the dissolved ozone could not be replenished in time, which affected the improvement of COD removal efficiency. At the same time, there was a certain degree of ozone loss due to its self-decomposition reaction since the system contained two-column. The disadvantages of SR were similar to TR. Moreover, the mass transfer efficiency was not as high as that of TR. Additionally, the two types of reactors needed two sets of reactor units, which made the volume utilization of the reactor inadequate. In the CR, the dissolved ozone in the catalyst bed could not be replenished in time. Additionally, due to the absence of catalytic reaction section at the bottom of the catalyst bed, the solution was quickly discharged from the reactor after passing through the catalyst layer, thereby leading to the decline of organic matter removal efficiency.

Table 4 shows the effect of the height of the ozone adsorption section on the COD removal efficiencies. With the increase of the height of the adsorption section (h_1) from 0.3 m to 1.69 m, COD removal efficiencies first increased and then decreased. When the height of the adsorption section (h_1) was 0.4 m, the highest COD removal efficiency was acquired. In this case, the ozone absorption section accounts for 19% of valid water depth (h) in the reactor. This value can be used as a reference parameter for the full-scale reactor design. When the height of the catalytic reaction section (h_3) was 0, the removal efficiency of COD was very low. It can be seen that the height of the catalytic reaction section (h_3) had a significant effect on the removal of organic matters, indicating that the indirect reaction would continue after the solution left the catalyst bed.

Table 4. Effect of structural parameters on the reactor performance.

Structural Parameters	h_1 , 0.30 m	h_1 , 0.40 m	h_1 , 0.80 m	h_1 , 1.69 m
	h_3 , 1.39 m	h_3 , 1.29 m	h_3 , 0.89 m	h_3 , 0 m
COD removal efficiency	45.6%	48.2%	47.5%	26.3%

Figure 7b shows an increase in circulation flow ratio (R) resulted in a decrease in $\Delta O_3/\Delta COD$ value and an increase in COD removal efficiency. When the R was increased from 250% to 300%, there was no significant improvement in COD removal efficiency. Additionally, a large circulation flow ratio would result in more operating costs due to the need for a higher power circulating pump. The overall apparent reaction rate constant by catalytic ozonation for COD removal was about 0.01 min^{-1} in the IR system with a circulation flow ratio of 250% and h_1 of 0.4 m. The overall apparent reaction rate constants in TR and SR were 0.0058 and 0.0047 min^{-1} , respectively. The results show an increase in the mass transfer efficiency resulted in an increase in the apparent reaction rate constant.

3.4. Removal of Organic Compounds with IR

Table 5 shows the results of the 16 PAHs present in the influent (BCW) and effluent samples for different running days. In the catalytic ozonation on day 15 of operation, the removal efficiencies of the 16 PAHs were more than 50%, most of which were more than 80%. Especially, acenaphthylene was not detected in the effluent. After 487 days of operation, no significant change in PAHs removal efficiency

was observed. Acenaphthylene was not detected in the effluent, either. The removal efficiencies of other PAHs were more than 50%. These results indicated that the stable removal efficiencies of PAHs were achieved by catalytic ozonation with the IR system. Although the removal efficiencies of PAHs decreased with the extension of the operation time, the concentration of PAHs in the effluent of 487 days still met the requirements of “the Emission Standard of Pollutants for Coking Chemical Industry in China” (GB 16171-2012). Our previous study [27] also showed that with the extension of the operation time, the effluent COD of 487 days still met the standard. The COD removal efficiencies on the 15th and 487th days were 58.5% and 51.4%, respectively. The corresponding effluent COD were 42.5 mg·L⁻¹ and 52.9 mg·L⁻¹, respectively. Thus, with the extension of the operation time, the removal efficiencies decreased but did not affect the removal of organic pollutants.

Table 5. The concentration of polycyclic aromatic hydrocarbons (PAHs) in the influent (BCW) and effluent samples for different running days.

	15 Day			487 Day		
	Influent (ug·L ⁻¹)	Effluent (ug·L ⁻¹)	Removal (%)	Influent (ug·L ⁻¹)	Effluent (ug·L ⁻¹)	Removal (%)
Naphthalene	0.5405	0.211	60.96	0.5523	0.2358	57.31
Acenaphthylene	0.3937	Not detected		0.3896	Not detected	
Acenaphthene	0.4125	0.0638	84.53	0.4345	0.0791	81.80
Fluorene	1.2784	0.1401	89.04	1.2788	0.1453	88.64
Phenanthrene	3.1121	0.3985	87.20	3.2136	0.4605	85.67
Anthracene	0.6121	0.1197	80.44	0.7089	0.1414	80.05
Fluoranthene	1.4787	0.2371	83.97	1.8129	0.3088	82.97
Pyrene	1.0649	0.1904	82.12	1.0742	0.1961	81.74
Benz[a]anthracene	0.2715	0.1218	55.14	0.2856	0.1314	53.99
Chrysene	0.1983	0.0751	62.13	0.2017	0.0778	61.43
Benzo[b]fluoranthene	0.3123	0.1358	56.52	0.3357	0.1488	55.67
Benzo[k]fluoranthene	0.2015	0.0944	53.15	0.2145	0.1022	52.35
Benzo[a]pyrene	0.0313	0.0133	57.51	0.0405	0.0179	55.80
Indeno[1,2,3-cd]pyrene	1.1235	0.1656	85.26	1.3257	0.2023	84.74
Dibenz[a,h]anthracene	1.9065	0.3752	80.32	2.0178	0.4395	78.22
Benzo[g,h,i]perylene	2.1321	0.2758	87.06	2.2456	0.3083	86.27

The UV254 removal efficiencies on day 15 and 487 of operation were 87% and 82%, respectively, indicating the stable oxidation efficiency for unsaturated organic compounds [38,39]. Additionally, the 3DEEM data were obtained during the full-scale application of the IR setup. The 3DEEM data of influent (i.e., BCW) had little change at different operation periods since the influent quality changed slightly in the full-scale operation. However, the 3DEEM spectrum of the effluent on day 487 was radically different from that of day 15. There were no peaks in the 3DEEM fluorescence of the effluent on day 15, as shown in Figure 8a. For the effluent on day 487 of operation, there was a weak signal of peak I (Figure 8b), which was related to fulvic acid-like aromatic substance [40], indicating that a small amount of fulvic acid-like aromatic substance existed in the effluent. There was some decline in the removal efficiency with the long-term operation, but the effluent could still meet the discharge standard without being affected. Thus, the process with the IR reactor is worth promoting. Based on the results from the long-term continuous catalytic ozonation with the full-scale IR system, the electricity charge, the liquid oxygen consumption cost, and the catalyst depreciation expense per ton of wastewater was USD 0.1402, USD 0.132, and USD 0.0084, respectively. Here, the unit price of the electricity, the liquid oxygen, and the catalyst was USD 0.1 (kW·h)⁻¹, USD 0.11 kg⁻¹, and USD 1.22 kg⁻¹, respectively. Thus, the operation cost per ton of wastewater was USD 0.2806, which was only 1/3–1/2 of that for the Fenton process.

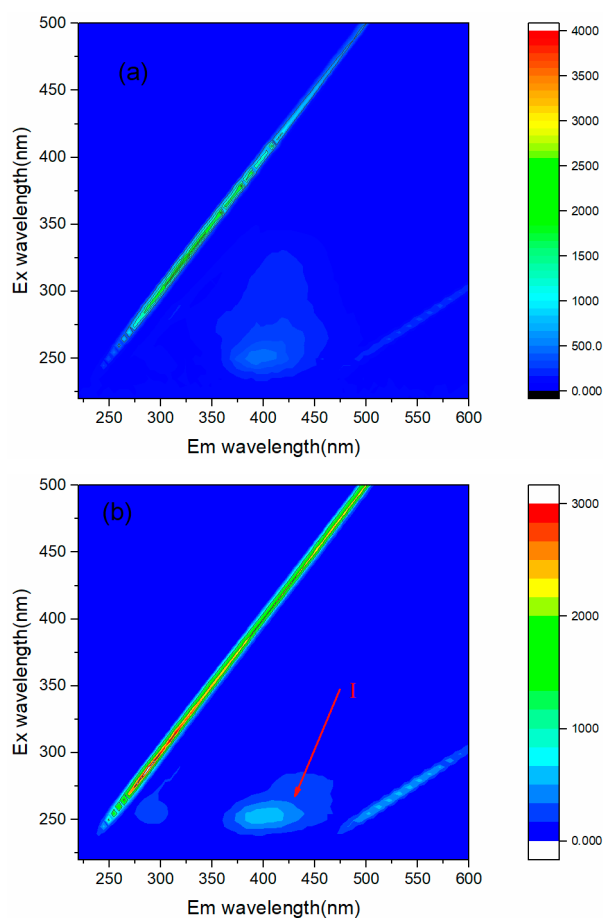


Figure 8. The 3DEEM spectrum for effluent from IR catalytic ozonation on (a) day 15 and (b) day 487.

4. Conclusions

The treatment of bio-treated coking wastewater (BCW) by catalytic ozonation system was investigated in semi-batch and continuous flow reactors using a practicable shell-core milli-sphere $Mn_xCe_{1-x}O_2/\gamma-Al_2O_3$ catalyst. Compared with single ozonation, the catalytic ozonation system exhibited an excellent degradation efficiency of organic pollutants in the BCW from the five coking plants. The COD removal efficiency after 120 min of catalytic reaction could reach 64–74%, but only 14.5–20% for single ozonation. The overall apparent reaction rate constants by catalytic ozonation and via single ozonation for COD removal were $0.0101\text{--}0.0117\text{ min}^{-1}$ and 0.0034 min^{-1} , respectively. The apparent reaction rate constant has no obvious correlation with the initial COD concentration of BCW and pre-treatment biological process. However, it increases with the improvement of the mass transfer efficiency of the reaction system. An integral reactor with catalytic ozonation stacked by ozone absorption (IR) demonstrated significantly better performance than other reactors in the continuous flow mode for the treatment of BCW. The mass transfer and the utilization efficiency of ozone were enhanced in the IR setup. The optimal ratio for the height of the adsorption section (h_1) to valid water depth (h) in the reactor and the optimal circulation flow ratio (R) was 19% and 250% for the IR setup, respectively. The long-term full-scale application demonstrated that the IR system exhibited a stable removal efficiency for PAHs in the BCW. The novel integral reactor (IR) can improve the process efficiency in the treatment of BCW by catalytic ozonation. The ratio of the height of the adsorption section (h_1) to valid water depth (h) in the reactor and the kinetics rate constants established in this work is helpful for the design and operation of the catalytic ozonation process. This study will promote the engineering application of the catalytic ozonation for the treatment of industrial

wastewater. We will focus on the improvement of the ozone aeration system and the research of the novel reactor mathematical model in the next step.

Author Contributions: Conceptualization, C.H. and J.W.; Data curation, C.H. and J.W.; Formal analysis, C.H. and H.X.; Funding acquisition, J.W.; Investigation, C.H., X.J., W.W. and X.X.; Methodology, C.H., J.W. and H.X.; Project administration, C.H. and J.W.; Resources, J.W.; Supervision, J.W.; Validation, J.W., H.X., X.J., W.W. and X.X.; Visualization, C.H.; Writing—original draft, C.H.; Writing—review and editing, C.H., J.W. and H.X. All authors have read and agreed to the published version of the manuscript.

Funding: The authors greatly appreciate the financial support from National Natural Science Foundation of China [Project no. 51978658].

Conflicts of Interest: The authors declare no conflict of interest.

References

1. Sharma, N.K.; Philip, L. Combined biological and photocatalytic treatment of real coke oven wastewater. *Chem. Eng. J.* **2016**, *295*, 20–28. [[CrossRef](#)]
2. Lai, P.; Zhao, H.-Z.; Zeng, M.; Ni, J.-R. Study on treatment of coking wastewater by biofilm reactors combined with zero-valent iron process. *J. Hazard. Mater.* **2009**, *162*, 1423–1429. [[CrossRef](#)] [[PubMed](#)]
3. Zhu, X.; Ni, J.; Lai, P. Advanced treatment of biologically pretreated coking wastewater by electrochemical oxidation using boron-doped diamond electrodes. *Water Res.* **2009**, *43*, 4347–4355. [[CrossRef](#)] [[PubMed](#)]
4. Sun, G.; Zhang, Y.; Gao, Y.; Han, X.; Yang, M. Removal of hard COD from biological effluent of coking wastewater using synchronized oxidation-adsorption technology: Performance, mechanism, and full-scale application. *Water Res.* **2020**, *173*. [[CrossRef](#)] [[PubMed](#)]
5. Ghuge, S.P.; Saroha, A.K. Catalytic ozonation for the treatment of synthetic and industrial effluents—Application of mesoporous materials: A review. *J. Environ. Manag.* **2018**, *211*, 83–102. [[CrossRef](#)]
6. Li, X.; Zhang, W.; Lai, S.; Gan, Y.; Li, J.; Ye, T.; You, J.; Wang, S.; Chen, H.; Deng, W.; et al. Efficient organic pollutants removal from industrial paint wastewater plant employing Fenton with integration of oxic/hydrolysis acidification/oxic. *Chem. Eng. J.* **2018**, *332*, 440–448. [[CrossRef](#)]
7. Li, K.; Yediler, A.; Yang, M.; Schulte-Hostede, S.; Wong, M.H. Ozonation of oxytetracycline and toxicological assessment of its oxidation by-products. *Chemosphere* **2008**, *72*, 473–478. [[CrossRef](#)]
8. Nawrocki, J.; Kasprzyk-Hordern, B. The efficiency and mechanisms of catalytic ozonation. *Appl. Catal. B Environ.* **2010**, *99*, 27–42. [[CrossRef](#)]
9. Dar, A.A.; Wang, X.; Wang, S.; Ge, J.; Shad, A.; Ai, F.; Wang, Z. Ozonation of pentabromophenol in aqueous basic medium: Kinetics, pathways, mechanism, dimerization and toxicity assessment. *Chemosphere* **2019**, *220*, 546–555. [[CrossRef](#)]
10. Zhang, T.; Croué, J.-P. Catalytic ozonation not relying on hydroxyl radical oxidation: A selective and competitive reaction process related to metal–carboxylate complexes. *Appl. Catal. B Environ.* **2014**, *144*, 831–839. [[CrossRef](#)]
11. Li, S.; Tang, Y.; Zhang, J.; Hao, W.; Chen, W.; Gu, F.; Hu, Z.; Li, L. Advanced and green ozonation process for removal of clofibric acid in water system: Preparation and mechanism analysis of efficient copper-substituted MCM-48. *Sep. Purif. Technol.* **2019**, *211*, 684–696. [[CrossRef](#)]
12. Yuan, L.; Shen, J.; Yan, P.; Zhang, J.; Wang, Z.; Zhao, S.; Chen, Z. Catalytic ozonation of 4-chloronitrobenzene by goethite and Fe²⁺-modified goethite with low defects: A comparative study. *J. Hazard. Mater.* **2019**, *365*, 744–750. [[CrossRef](#)] [[PubMed](#)]
13. Chen, W.; Bao, Y.; Li, X.; Huang, J.; Tang, Y.; Li, L. Mineralization of salicylic acid via catalytic ozonation with Fe-Cu@SiO₂ core-shell catalyst: A two-stage first order reaction. *Chemosphere* **2019**, *235*, 470–480. [[CrossRef](#)] [[PubMed](#)]
14. Gomes, J.; Frasson, D.; Quinta-Ferreira, R.M.; Matos, A.; Martins, R.C. Removal of Enteric Pathogens from Real Wastewater Using Single and Catalytic Ozonation. *Water* **2019**, *11*, 127. [[CrossRef](#)]
15. Wu, J.; Ma, L.; Chen, Y.; Cheng, Y.; Liu, Y.; Zha, X. Catalytic ozonation of organic pollutants from bio-treated dyeing and finishing wastewater using recycled waste iron shavings as a catalyst: Removal and pathways. *Water Res.* **2016**, *92*, 140–148. [[CrossRef](#)] [[PubMed](#)]

16. Zhuang, H.; Han, H.; Hou, B.; Jia, S.; Zhao, Q. Heterogeneous catalytic ozonation of biologically pretreated Lurgi coal gasification wastewater using sewage sludge based activated carbon supported manganese and ferric oxides as catalysts. *Bioresour. Technol.* **2014**, *166*, 178–186. [[CrossRef](#)]
17. Li, C.; Jiang, F.; Sun, D.; Qiu, B. Catalytic ozonation for advanced treatment of incineration leachate using (MnO₂-Co₃O₄)/AC as a catalyst. *Chem. Eng. J.* **2017**, *325*, 624–631. [[CrossRef](#)]
18. Wang, J.; Bai, Z. Fe-based catalysts for heterogeneous catalytic ozonation of emerging contaminants in water and wastewater. *Chem. Eng. J.* **2017**, *312*, 79–98. [[CrossRef](#)]
19. Nawrocki, J. Catalytic ozonation in water: Controversies and questions. Discussion paper. *Appl. Catal. B Environ.* **2013**, *142*, 465–471. [[CrossRef](#)]
20. Martins, R.C.; Quinta-Ferreira, R.M. Catalytic ozonation of phenolic acids over a Mn–Ce–O catalyst. *Appl. Catal. B Environ.* **2009**, *90*, 268–277. [[CrossRef](#)]
21. Martins, R.C.; Quinta-Ferreira, R.M. Screening of Ceria-Based and Commercial Ceramic Catalysts for Catalytic Ozonation of Simulated Olive Mill Wastewaters. *Ind. Eng. Chem. Res.* **2009**, *48*, 1196–1202. [[CrossRef](#)]
22. Faria, P.C.; Monteiro, D.C.; Orfao, J.J.; Pereira, M.F. Cerium, manganese and cobalt oxides as catalysts for the ozonation of selected organic compounds. *Chemosphere* **2009**, *74*, 818–824. [[CrossRef](#)] [[PubMed](#)]
23. Zhang, T.; Chen, W.; Ma, J.; Qiang, Z. Minimizing bromate formation with cerium dioxide during ozonation of bromide-containing water. *Water Res.* **2008**, *42*, 3651–3658. [[CrossRef](#)]
24. Li, W.; Lu, X.; Xu, K.; Qu, J.; Qiang, Z. Cerium incorporated MCM-48 (Ce-MCM-48) as a catalyst to inhibit bromate formation during ozonation of bromide-containing water: Efficacy and mechanism. *Water Res.* **2015**, *86*, 2–8. [[CrossRef](#)] [[PubMed](#)]
25. Shan, C.; Xu, Y.; Hua, M.; Gu, M.; Yang, Z.; Wang, P.; Lu, Z.; Zhang, W.; Pan, B. Mesoporous Ce-Ti-Zr ternary oxide millispheres for efficient catalytic ozonation in bubble column. *Chem. Eng. J.* **2018**, *338*, 261–270. [[CrossRef](#)]
26. Wei, K.; Cao, X.; Gu, W.; Liang, P.; Huang, X.; Zhang, X. Ni-Induced C-Al₂O₃-Framework (NiCAF) Supported Core-Multishell Catalysts for Efficient Catalytic Ozonation: A Structure-to-Performance Study. *Environ. Sci. Technol.* **2019**, *53*, 6917–6926. [[CrossRef](#)] [[PubMed](#)]
27. He, C.; Wang, J.; Wang, C.; Zhang, C.; Hou, P.; Xu, X. Catalytic ozonation of bio-treated coking wastewater in continuous pilot- and full-scale system: Efficiency, catalyst deactivation and in-situ regeneration. *Water Res.* **2020**, *183*, 116090. [[CrossRef](#)] [[PubMed](#)]
28. Rakness, K.; Gordon, G.; Langlais, B.; Masschelein, W.; Matsumoto, N.; Richard, Y.; Robson, C.M.; Somiya, I. Guideline for Measurement of Ozone Concentration in the Process Gas from an Ozone Generator. *Ozone Sci. Eng.* **1996**, *18*, 209–229. [[CrossRef](#)]
29. Bader, H.; Hoigné, J. Determination of ozone in water by the indigo method. *Water Res.* **1981**, *15*, 449–456. [[CrossRef](#)]
30. Mahlaba, S.V.L.; Valand, J.; Mahomed, A.S.; Friedrich, H.B. A study on the deactivation and reactivation of a Ni/Al₂O₃ aldehyde hydrogenation catalyst: Effects of regeneration on the activity and properties of the catalyst. *Appl. Catal. B Environ.* **2018**, *224*, 295–304. [[CrossRef](#)]
31. Liu, Y.; Feng, Y.; Yao, J. Recent advances in the direct fabrication of millimeter-sized hierarchical porous materials. *RSC Adv.* **2016**, *6*, 80840–80846. [[CrossRef](#)]
32. Purwajanti, S.; Zhang, H.; Huang, X.; Song, H.; Yang, Y.; Zhang, J.; Niu, Y.; Meka, A.K.; Noonan, O.; Yu, C. Mesoporous Magnesium Oxide Hollow Spheres as Superior Arsenite Adsorbent: Synthesis and Adsorption Behavior. *ACS Appl. Mater. Inter.* **2016**, *8*, 25306–25312. [[CrossRef](#)] [[PubMed](#)]
33. Bing, J.; Hu, C.; Zhang, L. Enhanced mineralization of pharmaceuticals by surface oxidation over mesoporous γ -Ti-Al₂O₃ suspension with ozone. *Appl. Catal. B Environ.* **2017**, *202*, 118–126. [[CrossRef](#)]
34. Chen, H.; Sayari, A.; Adnot, A.; Larachi, F.L. Composition-activity effects of Mn–Ce–O composites on phenol wet oxidation. *Appl. Catal. B Environ.* **2001**, *32*, 195–204. [[CrossRef](#)]
35. Cargnello, M.; Delgado Jaen, J.J.; Hernandez Garrido, J.C.; Bakhmutsky, K.; Montini, T.; Calvino Gamez, J.J.; Gorte, R.J.; Fornasiero, P. Exceptional activity for methane combustion over modular Pd@CeO₂ subunits on functionalized Al₂O₃. *Science* **2012**, *337*, 713–717. [[CrossRef](#)] [[PubMed](#)]
36. Wang, J.; Xia, Z.; Cao, Z.; Yang, S.; Zhu, W. Mathematical model involving chemical reaction and mass transfer for the ozonation of dimethyl phthalate in water in a bubble column reactor. *J. Adv. Oxid. Technol.* **2017**, *20*. [[CrossRef](#)]

37. Huang, G.; Pan, F.; Fan, G.; Liu, G. Application of heterogeneous catalytic ozonation as a tertiary treatment of effluent of biologically treated tannery wastewater. *J Environ. Sci. Heal. A* **2016**, *51*, 626–633. [[CrossRef](#)]
38. Kasprzyk-Hordern, B.; Ziolek, M.; Nawrocki, J. Catalytic ozonation and methods of enhancing molecular ozone reactions in water treatment. *Appl. Catal. B Environ.* **2003**, *46*, 639–669. [[CrossRef](#)]
39. Maddila, S.; Dasireddy, V.D.B.C.; Jonnalagadda, S.B. Dechlorination of tetrachloro-o-benzoquinone by ozonation catalyzed by cesium loaded metal oxides. *Appl. Catal. B Environ.* **2013**, *138*, 149–160. [[CrossRef](#)]
40. Yang, W.; Li, X.; Pan, B.; Lv, L.; Zhang, W. Effective removal of effluent organic matter (EfOM) from bio-treated coking wastewater by a recyclable aminated hyper-cross-linked polymer. *Water Res.* **2013**, *47*, 4730–4738. [[CrossRef](#)]



© 2020 by the authors. Licensee MDPI, Basel, Switzerland. This article is an open access article distributed under the terms and conditions of the Creative Commons Attribution (CC BY) license (<http://creativecommons.org/licenses/by/4.0/>).